Carrier-mediated long-range ferromagnetism in electron-doped Fe-C_{4} and Fe-N_{4} incorporated graphene

Alex Taekyung Lee, Joongoo Kang, Su-Huai Wei, K. J. Chang, and Yong-Hyun Kim

Phys. Rev. B **86**, 165403 — Published 1 October 2012

DOI: 10.1103/PhysRevB.86.165403

Carrier-Mediated Long-Range Ferromagnetism in Electron-Doped Fe-C_4 and Fe-N_4 Incorporated Graphene

Alex Taekyung Lee,[1] Joongoo Kang,[2] Su-Huai Wei,[2] K. J. Chang,[1,*] and Yong-Hyun Kim[3,1,†]

[1]*Department of Physics, KAIST, Daejeon 305-701, Korea*

[2]*National Renewable Energy Laboratory, Golden, Colorado 80401, USA*

[3]*Graduate School of Nanoscience and Technology (WCU) and KAIST Institute for the NanoCentury, KAIST, Daejeon 305-701, Korea*

(Received: September 21, 2012)

Abstract

Graphene magnetism has been proposed but based on thermodynamically unstable zigzag edges and dangling electrons with broken sublattice symmetry. From results of first-principles calculations, we propose a way to realize thermodynamically stable graphene ferromagnetism by seamlessly incorporating transition metals into the graphene honeycomb network. An Fe atom substituting a carbon-carbon dimer of graphene can result in nearly square-planar covalent bonding between the spin-polarized Fe 3*d* orbitals and graphene dangling bond states. Dangling bond passivation of the divacancy pore with N and O strongly affects the Fe incorporation into the graphene network in terms of energetics and electronic structure. The Fe-N_4 or Fe-C_4 incorporated graphene is predicted to show long-range ferromagnetism particularly due to carrier mediation when electron doped.

* Corresponding Author: kchang@kaist.ac.kr

† Corresponding Author: yong.hyun.kim@kaist.ac.kr

As carbon is durable, light, and abundant, carbon-based magnets are expected to be more stable, versatile, and inexpensive than the current transition-metal-based magnets. Among the various carbon materials, magnetism in graphene has been extensively studied for its potential use for novel spin/electronics devices relying on the unique electronic structure of graphene [1-4]. However, graphene magnetism based on zigzag edges with single H termination (z_1) is almost inapplicable not only because of the difficulty to make the well-defined zigzag edges, but also because the z_1 termination seems not thermodynamically stable compared to non-magnetic z_{112} termination (with two sp^2 and one sp^3 terminations) under terrestrial thermodynamics condition [5]. Experimentally it has been reported that pristine graphene shows no intrinsic ferromagnetism even when the temperature goes down to 2 K and only exhibits diamagnetism [6].

Intrinsic and extrinsic defects in graphene, e.g., vacancies [7,8], H or F sp^3-functionalization [9-11], and transition metals [12-16], can be a source of magnetism by generating dangling bond (DB) states. Particularly, it is theoretically proposed that H- or F-functionalized graphene could exhibit local magnetism only when the graphene sub-lattice symmetry is broken [9-11]. The sp^3-functionalized carbon results in one DB with 1 Bohr-magneton (μ_B). However, DB-based extensive ferromagnetism may not be feasible because the DB states are generally unstable. Extrinsic transition metal (TM) defects in graphene can be a good candidate for practical realization of graphene magnetism with large magnetic moment, but it is not well understood (1) if the TM defects would be thermodynamically stable and (2) if TM incorporation could cause any DB in graphene electronic structure. Very recently, it has been demonstrated that TM-divacancy complexes [12,13] are more stable thermodynamically than previously-proposed TM-monovacancy complexes [14-16] in graphene.

Here we report the results of first-principles density functional theory calculations for the

thermodynamic stability and electronic and magnetic properties of Fe-divacancy complex incorporated graphene, in which a carbon-carbon dimer is replaced by an Fe atom [12,13]. Because oxygen and nitrogen are common impurities in graphene as well [17-19], we examine the stability of Fe impurities surrounded by various combinations of C, N, and O at the divacancy pore. Whereas the O treatment almost self-passivates the DBs of the divacancy pore with yielding weak Fe adsorption, the tight-bonded Fe-C_4 complex is yet DB rich with being electron deficient. The biomimetic Fe-N_4 complex is most stable thermodynamically with almost exact DB passivation. Our first-principles calculations show that the Fe-C_4 and Fe-N_4 complexes can be aligned ferromagnetically in graphene with > 2 μ_B/Fe, particularly when electron doped. The long-range ordering of the local magnetic moment in graphene can be attributed to the π-electron mediation after the *p*-*d* orbital coupling.

For atomic and electronic structure analyses of Fe-incorporated graphene, we performed spin-polarized density-functional theory (DFT) calculations using the projector-augmented wave potentials [20] and Perdew-Burke-Ernzerhof [21] functional as implemented in the Vienna Ab-initio Simulation Package (VASP) [22]. The wave functions were expanded in plane waves with a kinetic energy cutoff of 500 eV. We mostly used a 4×4 graphene supercell with a vacuum region of 15 Å for ferromagnetic Fe impurities in graphene. The 8×8 supercell calculations ensured that the calculated formation energies were accurate to within 0.1 eV. We employed a **k**-point set generated by the 12×12×1 Monkhorst-Pack mesh. The pairwise magnetic coupling was analyzed in the 8×8 supercell. All atomic coordinates were optimized until the residual forces were less than 0.015 eV/ Å.

When a single Fe atom is adsorbed on perfect graphene, the adsorption energy (0.75 eV) [23] is much smaller than the cohesive energy (4.28 eV) of bulk Fe, so that adsorbed Fe atoms tend to aggregate. In the presence of a carbon monovacancy, the Fe adsorption energy at the defect site increases to about 7 eV [15], which is large enough to prevent aggregation.

An Fe adatom also interacts strongly with a carbon divacancy with the adsorption energy of 6 eV [15]. Note that the above adsorption energies are all referenced to the reactive atomic Fe.

Very recently it is reported that Fe forms a very stable Fe-N_4 porphyrin-like moiety in graphene [12,13] when the four C atoms surrounding the divacancy pore are substituted by nitrogen. The rectangular divacancy pore can be chemically modified in various combinations of C, N, and O. We investigated the energetics and magnetic characteristics of Fe-incorporated $C_lN_mO_n$ divacancy pores, where l, m, and n are the numbers of C, N, and O around the divacancy, respectively, whose sum is 4. Figure 1 shows three representative Fe-C_4, Fe-N_4, and Fe-O_4 complexes incorporated into graphene. The almost-planar Fe atom is slightly protruded from the graphene plane by 0.49, 0.03, and 0.67 Å in the C_4, N_4, and O_4 pores, respectively. The protrusion of Fe indicates that Fe fits best to the N_4 pore. Note that the Fe protrusion in the O_4 pore is largest in spite of the smallest ionic size of O. This is attributed to the self-passivation of the O_4 pore, and thus to weak physisorption of Fe at the pore, as we will discuss shortly.

The formation energies of various $C_lN_mO_n$ divacancy pores were calculated by using the formula [24], $E_{\text{form}}(C_lN_mO_n) = E(C_lN_mO_n) - E(\text{graphene}) - (l-6)\mu_C - m\mu_N - n\mu_O$, where $E(C_lN_mO_n)$ and E(graphene) are the DFT total energies of the supercell containing a $C_lN_mO_n$ pore and pristine graphene, respectively. The chemical potentials μ_i (i = C, N, O) are taken from pristine graphene, N_2, and O_2 gas molecules, respectively [24]. We also calculated the formation energies of Fe-$C_lN_mO_n$ complexes, which are defined as, $E_{\text{form}}(\text{Fe-}C_lN_mO_n) = E(\text{Fe-}C_lN_mO_n) - E(\text{graphene}) - (l-6)\mu_C - m\mu_N - n\mu_O - \mu_{Fe}$, where μ_{Fe} is the Fe chemical potential obtained from body-centered cubic (bcc) Fe. The energy difference, $E_{\text{form}}(C_lN_mO_n) - E_{\text{form}}(\text{Fe-}C_lN_mO_n)$, actually represents the Fe binding energy at the pore site with reference to the cohesive energy of bcc Fe.

Among the $C_lN_mO_n$ divacancy pores, the O_4 pore has the lowest formation energy due to

the self-passivation of DBs by the epoxy-like O, as shown in Fig. 1(d). On the other hand, the formation energy of the C_4 pore is highest because the C DBs are not passivated at all even after the small C-C reconstruction. The DBs of the N_4 pore should be less reactive than those of the C_4 pore because of the partial C DB passivation by N, so that its formation energy lies in between the O_4 and C_4 pores. Yet, the N_4 pore is not completely passivated. The remaining DBs of the N_4 pore act as a (–2) anion according to our electronic structure analysis [12,13], similar to N_4-macrocycles such as porphyrin and phthalocyanine. The stability of Fe-$C_lN_mO_n$ complexes is determined by the interaction between the Fe and the leftover DBs in the pore. Because Fe can be a divalent cation in the planar geometry, the best-matched $Fe^{(2+)}$-$N_4^{(2-)}$ complex has the lowest formation energy, as shown in Fig. 1(e). The Fe binding energy to the pore is highest for Fe-CN_3 with falling into the covalent bonding regime, whereas it is lowest for Fe-O_4 with falling into the physisorption regime [Fig. 1(f)]. The negative binding energies of Fe for the O-rich pores indicate that the Fe complex formation at the O-rich pores is highly unlikely over Fe cohesion. While the Fe-N_4 complex is most likely to exist – as also confirmed by experiment [12], metastable Fe-divacancy complexes in the C-rich pores can kinetically coexist [13] due to their high binding energies [Fig. 1(f)]. The above formation energetics could be generally applicable for other divalent TMs incorporated into divacancy pores of graphene. We note that the binding energies of Fe-C_4 and Fe-N_4 are consistent with the previously reported results when the atomic Fe is used for μ_{Fe} [13,15].

We examined the electronic structure of Fe-X_4 (X=C, N, O) complexes in graphene to understand the variations of the formation and binding energies in Fig. 1(d)-1(f). The total and projected densities of states (DOS) onto the Fe *d* and X_4-pore *p* orbitals are presented in Fig. 2, together with the total DOS of pristine graphene. In the Fe-C_4 complex [Fig. 2(a)], the Fe $d_{x^2-y^2}$ orbitals strongly interact with the C_4 *p* orbitals, resulting in the high antibonding $d_{x^2-y^2}$ level. This strong covalency is the origin of the high binding energy of Fe at the C_4 pore in

Fig. 1(f). It is noted that Fe-C_4 incorporated graphene is slightly hole-doped, as shown in the band alignment; the Fermi level is lower than the graphene Dirac point. To fully passivate the C_4 DBs, about 5.3 (=4/3×4) electrons are required. Figure 2(a) shows that the Fe atom provides about three valence electrons to passivate the DBs. The yet electron-thirsty C_4 pore should withdraw some π-electrons from graphene to passivate its remaining DBs, leading to the hole doping to the host graphene. The projected DOS shows that the central Fe has approximately 4 spin-up and 1 spin-down electrons, whereas the peripheral C_4 carries additional spin-up electrons, yielding the net magnetic moment of ~3.6 μ_B, which is similar to the previous result [15]. The Fe-N_4 complex also exhibits the covalent p-$d_{x^2-y^2}$ hybridization [Fig. 2(b)], but the Fe d bands are less broadened than in the Fe-C_4 case. The Fermi level is located almost at the Dirac point, indicating no DB remains. The Fe is in the d^6 configuration with 4 spin-up and 2 spin-down electrons, as in the Fe-porphyrin molecule [12,13,25]. In the Fe-O_4 complex, the Fe atom weakly interacts with the self-passivated pore. Because the atom-like Fe donates one electron to graphene, graphene DOS appears slightly electron-doped [Fig. 2(c)]. The weakly ionized Fe causes the large Fe protrusion in the self-passivated O_4 pore.

Graphene in general can be doped with electrons and holes easily via unintentional charge transfer doping or intentional gate doping. Also, because of the incompletely passivated DBs in the electron-deficient Fe-C_4, it is expected that the Fe-C_4 defect is likely to be electron doped. Figure 3(a)-3(b) show the formation energies of charged Fe-N_4 and Fe-C_4 defects as a function of the Fermi level. The stability of charged defects varies with the chemical potential [24]. The Dirac point of the graphene is set to energy zero. The neutral Fe-N_4 is most stable near the Dirac point from –0.8 to 1.2 eV. When the Fermi level is raised greater than 1.2 eV, it can be negatively charged by one electron. On the other hand, neutral Fe-C_4 is most stable from –1.5 to 0.4 eV. It can be negatively charged rather easily than Fe-N_4. Because graphene

is metallic, it can be also charged fractionally. So, if we dope Fe-C_4 by 0.5 electrons, the formation energy of the charged state is –30 meV lower than that of the neutral state at the Dirac point, as shown in Fig. 3(b). This is consistent with the fact that Fe-C_4 incorporated graphene is hole-doped due to incompletely passivated DBs.

To see a possibility of the ferromagnetic arrangement of the thermodynamically stable Fe-N_4 and kinetically accessible Fe-C_4 defects in graphene with magnetic moments > 2 μ_B per site, we calculated the energy difference between the ferromagnetic (FM) and anti-ferromagnetic (AFM) configurations, i.e., $\Delta E = E(\text{AFM}) - E(\text{FM})$ of two Fe-X_4 defects separated by an Fe-Fe distance (d) in graphene. Noticeably the FM-AFM stability in Fig. 3(c) shows an oscillation as a function of d without any strong dependency on direction. Recently, it has been reported that the magnetic interactions between two substitutional Co atoms are ferromagnetic for the same sublattice sites, while they are antiferromagnetic or spin compensated for the different sublattice sites [16]. H- or F-functionalized graphene exhibits similar magnetic interactions [9-11]. However, Fe-X_4 defects do not intrinsically exhibit such a sublattice dependency because the defects perturb both the sublattices of graphene symmetrically. Due to the strong $p(\pi)$-d hybridization in Fe-C_4, the Fe-Fe interaction is more prominent for Fe-C_4 than for Fe-N_4.

The FM state is greatly stabilized to a long range for negatively-charged Fe-N_4 and Fe-C_4 defects although the oscillation feature is somewhat remained, as shown in Fig. 3(d). The FM stabilization can be understood by the band coupling model of the hybridized d_{z^2} state with graphene π states [26], as shown in Fig. 4(a). For the neutral Fe-N_4 and Fe-C_4 defects, the spin-up d_{z^2} state is fully occupied by electron, and the spin-down d_{z^2} state is empty. This neutral electronic configuration generally favors the AFM state according to the band coupling model [26]. On the other hand, when the system is e fractionally electron doped and thus the spin-down d_{z^2} state is partially occupied by α, as shown in Fig. 4(a), the FM state can

be favored via carrier-mediated double exchange mechanism, which is well known in dilute magnetic semiconductors [27]. According to the band coupling model, the FM coupling leads to an energy gain of $-2\alpha\Delta_{22}$, where Δ_{22} is the direct-exchange level splitting, and the AFM coupling yields the energy gain of $-2(1-\alpha)\Delta_{12}$, where Δ_{12} is the superexchange level splitting. Then, the FM-AFM stabilization energy $\Delta E = E(\mathrm{AFM}) - E(\mathrm{FM}) = 2\alpha(\Delta_{22} + \Delta_{12}) - 2\Delta_{12}$. Thus if $\alpha \geq \Delta_{12} / (\Delta_{22} + \Delta_{12}) = \alpha_c$, the FM state would be preferred. In general, α_c is smaller than 0.5 because Δ_{12} is smaller than Δ_{22}. By doping 1 electron to Fe-C_4 and Fe-N_4 complexes, the hybridized d_{z2} state is partially occupied more than half, as shown in Fig. 4(b) and 4(c), so that their FM states are stabilized to a long range.

In conclusion, from first-principles calculations we have investigated thermodynamic stability and ferromagnetism of Fe-X_4 divacancy complexes in graphene, in which the divacancy pore is chemically modified with N and O. We have found that kinetically accessible Fe-C_4 and thermodynamically stable Fe-N_4 complexes can result in a long-range ferromagnetism when electron doped. Our finding could be readily generalized for other transition metals incorporated into the divacancy in graphene and thus for understanding their magnetic properties. Also, the proposed ferromagnetism in Fe-incorporated graphene can be utilized for designing graphene/TM and carbon nanotube/TM based spin electronics devices such as spin filter [28] and magnetoresistance device [29].

Acknowledgement: This work was supported by the WCU program (R31-2008-000-10071-0) and Basic Science Research program (2010-0006922) through the National Research Foundation of Korea (NRFK). A.T.L and K.J.C. acknowledge the support by NRFK under Grant No. NRF-2011-0093845. The work at NREL is funded by the U.S. DOE and NREL LDRD programs under Grant No. DE-AC36-08GO28308.

Figure 1: Atomic structures of (a) Fe-C_4, (b) Fe-N_4, and (c) Fe-O_4 complexes in graphene. Formation energies (in unit of eV) of (d) chemically modified divacancy pores [$E_{form}(C_lN_mO_n)$] and (e) Fe-divacancy complexes [E_{form}(Fe-$C_lN_mO_n$)], and (f) binding energies defined as $E_{form}(C_lN_mO_n) - E_{form}$(Fe-$C_lN_mO_n$).

Figure 2: Total and projected densities of states (DOS) of (a) Fe-C_4, (b) Fe-N_4, and (c) Fe-O_4 complexes in graphene, as compared to the total DOS (dotted lines) of pristine graphene. Red and blue lines represent the projected DOS onto the Fe *d* and pore *p* orbitals, respectively, which are four times enlarged for clarity. The vertical dashed lines denote the Fermi energy. The insets show the DOS near the Dirac point. The energy zero indicates the vacuum level.

Figure 3: Formation energies of (a) Fe-N_4 and (b) Fe-C_4 complexes in graphene with different charged states of (+1), (0), and (–1). For the Fe-C_4 case, the (–0.5) charged state is also considered. Total energy differences (ΔE) between the FM and AFM states as a function of the Fe-Fe distance (*d*) for (c) neutral and (d) negatively-charged Fe-C_4 and Fe-N_4 complexes. The inset of (c) shows two Fe-N_4 embedded configurations considered. When one Fe atom is located at the center of the graphene, the other Fe positions represented by red and blue segments indicate the FM and AFM interactions, respectively.

Figure 4: (a) Charge density plot for the hybridized d_{z2} state in Fe-C_4 and its FM and AFM band coupling models. Because of the hybridized state, two distance Fe atoms can efficiently couple electronically. Total (black) and projected (red) DOS onto the Fe *d* for the (–1) charged (b) Fe-N_4 and (c) Fe-C_4. The projected DOS onto the Fe *d* is enlarged four times for clarity.

References

1. N. Tombros, C. Jozsa, M. Popinciuc, H. T. Jonkman, and B. J. van Wees, Nature (London) **448**, 571 (2007).
2. O. V. Yazyev and M. I. Katsnelson, Phys. Rev. Lett. **100**, 047209 (2008).
3. W. Han, K. Pi, K. M. McCreary, Y. Li, J. J. I. Wong, A. G. Swartz, and R. K. Kawakami, Phys. Rev. Lett. **105**, 167202 (2010).
4. Y.-W. Son, M. L. Cohen, and S. G. Louie, Nature (London) **444**, 347 (2006).
5. T. Wassmann, A. P. Seitsonen, A. M. Saitta, M. Lazzeri, and F. Mauri, Phys. Rev. Lett. **101**, 096402 (2008).
6. M. Sepioni, R. R. Nair, S. Rablen, J. Narayanan, F. Tuna, R. Winpenny, A. K. Geim, and I. V. Grigorieva, Phys. Rev. Lett. **105**, 207205 (2010)
7. P. Esquinazi, D. Spemann, R. Höhne, A. Setzer, K. -H. Han, and T. Butz, Phys. Rev. Lett. **91**, 227201 (2003).
8. J. Červenka, M. I. Katsnelson, and C. F. J. Flipse, Nature Phys. **5**, 840 (2009).
9. O. V. Yazyev, Phys. Rev. Lett. **101**, 037203 (2008).
10. T. O. Wehling, M. I. Katsnelson, and A. I. Lichtenstein, Phys. Rev. B **80**, 085428 (2009).
11. R. R. Nair, M. Sepioni, I.-L. Tsai, O. Lehtinen, J. Keinonen, A. V. Krasheninnikov, T. Thomson, A. K. Geim, and I. V. Grigorieva, Nature Phys. **8**, 199 (2012).

12. D. H. Lee, W. J. Lee, W. J. Lee, S. O. Kim, and Y.-H. Kim, Phys. Rev. Lett. **106**, 175502 (2011).

13. W. I. Choi, S.-H. Jhi, K. Kim, and Y.-H. Kim, Phys. Rev. B **81**, 085441 (2010).

14. R. Sielemann, Y. Kobayashi, Y. Yoshida, H. P. Gunnlaugsson, and G. Weyer, Phys. Rev. Lett. **101**, 137206 (2008).

15. A. V. Krasheninnikov, P. O. Lehtinen, A. S. Foster, P. Pyykkö, and R. M. Nieminen, Phys. Rev. Lett. **102**, 126807 (2009).

16. E. J. G. Santos, D. Sánchez-Portal, and A. Ayuela, Phys. Rev. B **81**, 125433 (2010).

17. G. E. Hammer and L. T. Drzal, Appl. Surf. Sci. **4**, 340 (1980).

18. W. S. Hummers. Jr. and R. E. Offeman, J. Am. Chem. Soc. **80**, 1339 (1958).

19. D. Wei, Y. Liu, Y. Wang, H. Zhang, L. Huang, and G. Yu, Nano Lett. **9**, 1752 (2009).

20. P. E. Blöchl, Phys. Rev. B **50**, 17953 (1994).

21. J. P. Perdew, K. Burke, and M. Ernzerhof, Phys. Rev. Lett. **77**, 3865 (1996).

22. G. Kresse and D. Joubert, Phys. Rev. B **59**, 1758 (1999).

23. K. T. Chan, J. B. Neaton, and M. L. Cohen, Phys. Rev. B **77**, 235430 (2008).

24. S. B. Zhang and J. E. Northrup, Phys. Rev. Lett. **67**, 2339 (1991).

25. Y.-H. Kim, Y. Y. Sun, W. I. Choi, J. Kang, and S. B. Zhang, Phys. Chem. Chem. Phys. **11**, 11400 (2009).

26. G. M. Dalpian and S.-H. Wei, Phys. Stat. Sol. B **243**, 9, 2170 (2006).

27. K. Sato, L. Bergqvist, J. Kudrnovský, P. H. Dederichs, O. Eriksson, I. Turek, B. Sanyal, G. Bouzerar, H. Katayama-Yoshida, V. A. Dinh, T. Fukushima, H. Kizaki, and R. Zeller, Rev. Mod. Phys. **82**, 1633 (2010).

28. Y. Yang, Y. Xiao, W. Ren, X. H. Yan, and F. Pan, Phys. Rev. B **84**, 195447 (2011).

29. J. M. de Almeida, A. R. Rocha, A. J. R. da Silva, and A. Fazzio, Phys. Rev. B **84**, 085412 (2011).

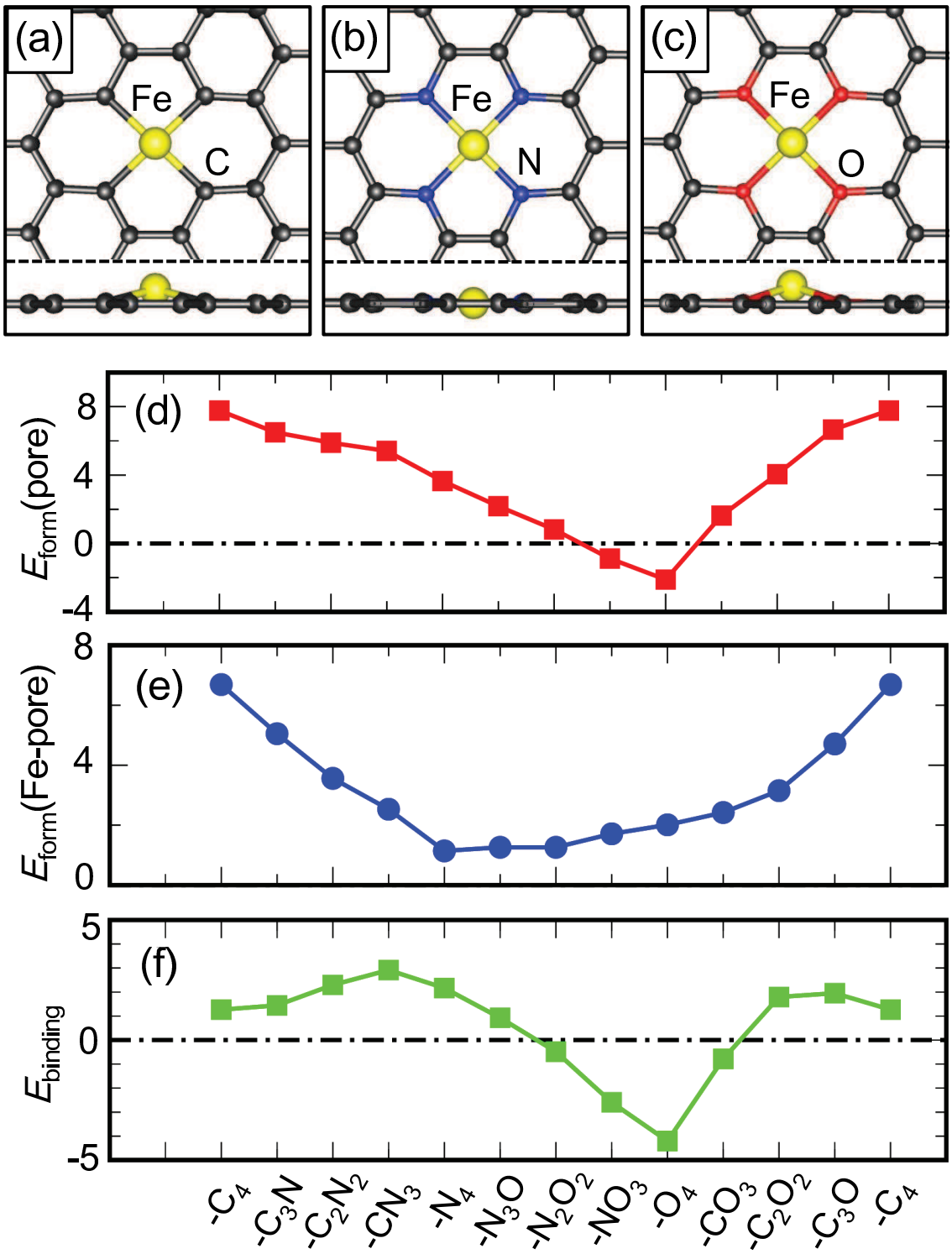

Figure 1 LL12931B 21SEP2012

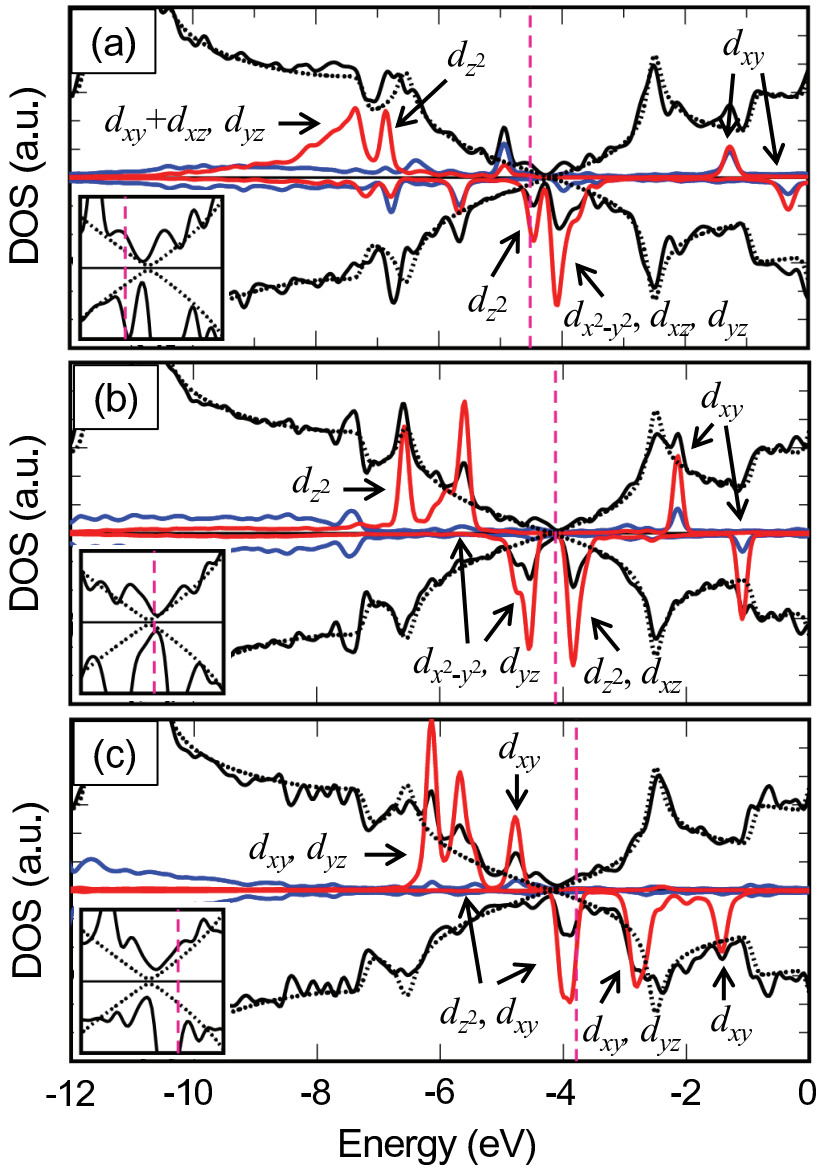

Figure 2 LL12931B 21SEP2012

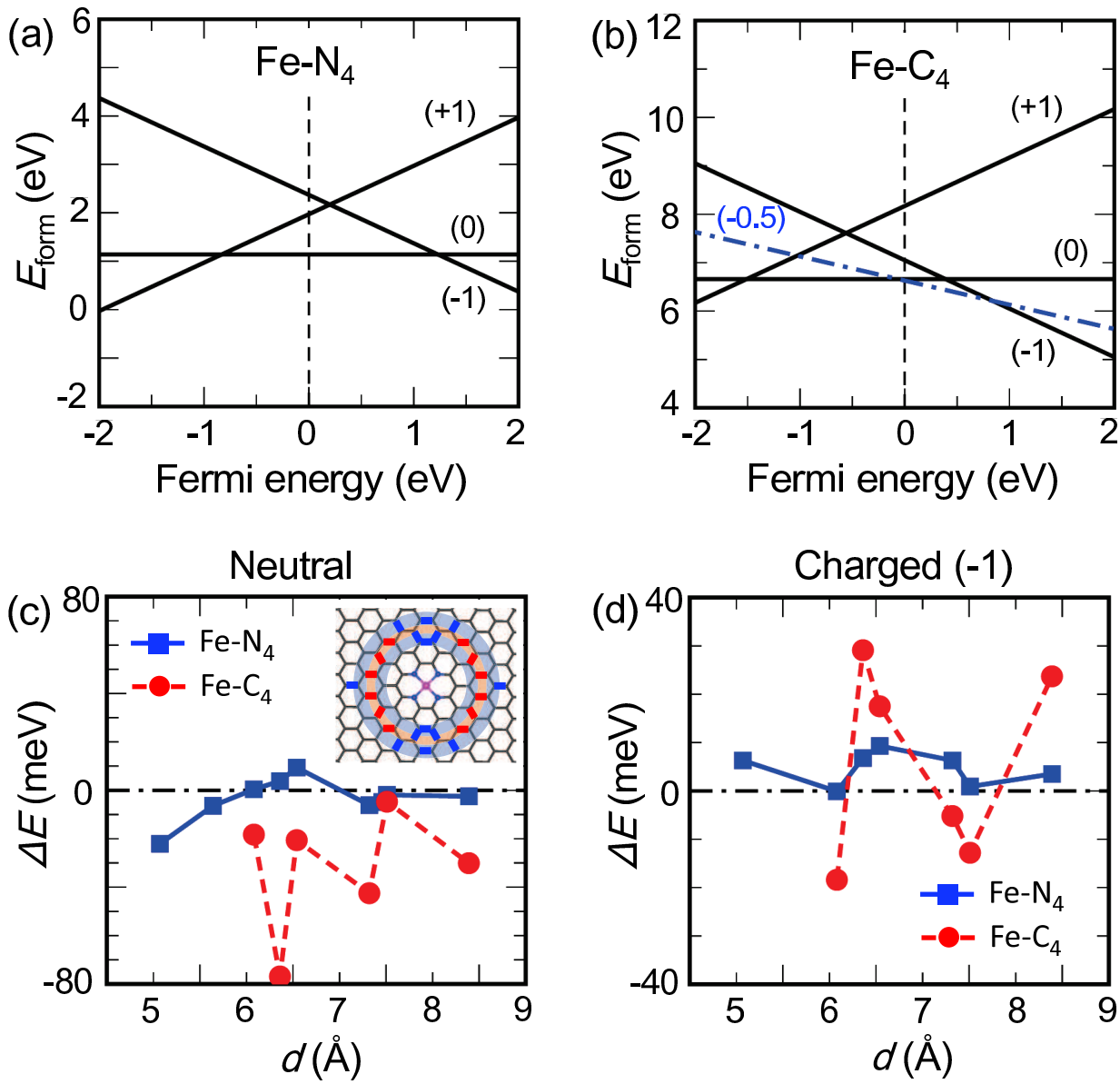

Figure 3 LL12931B 21SEP2012

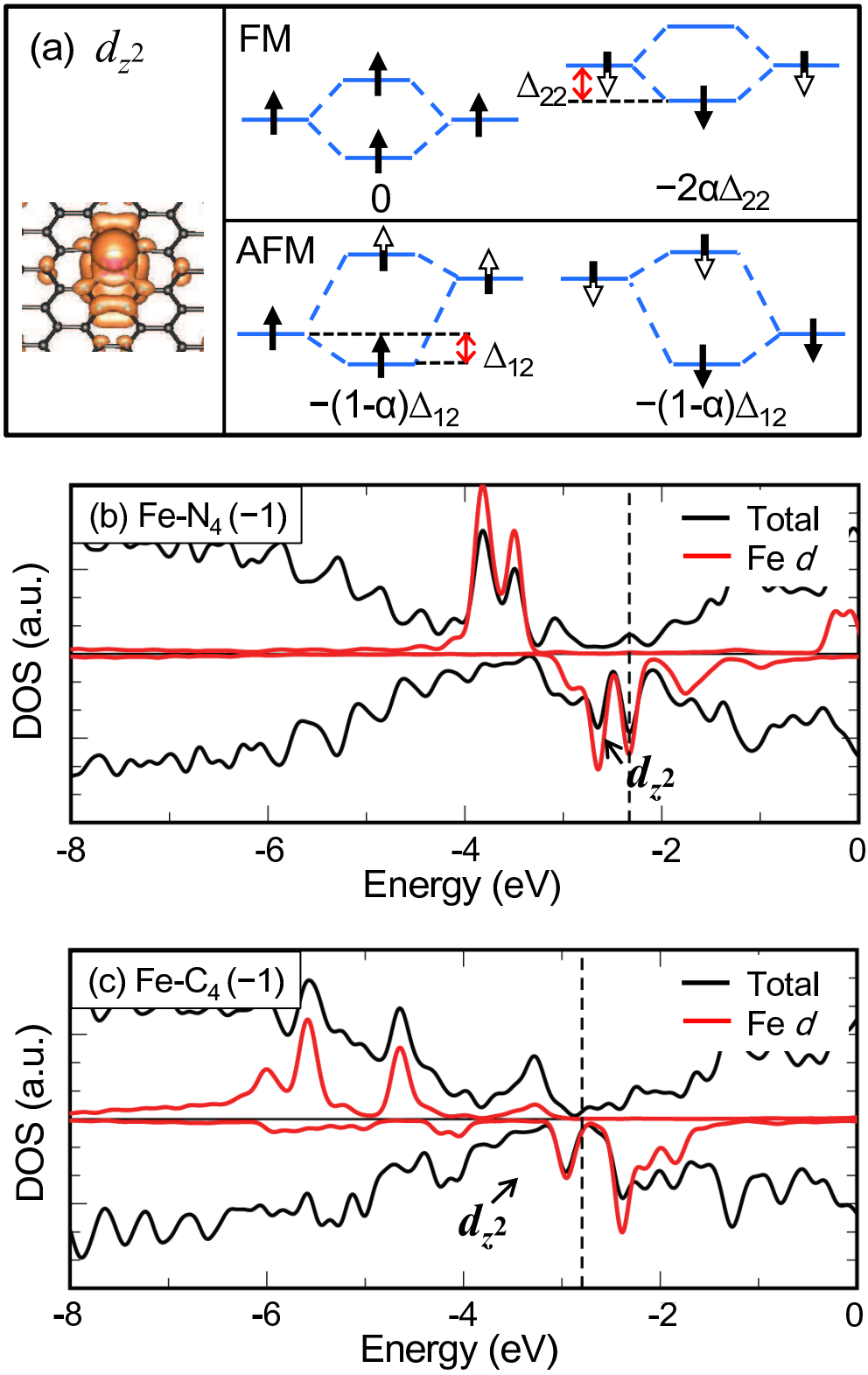

Figure 4 LL12931B 21SEP2012